Stable atomic structure of NiTi austenite

Nikolai A. Zarkevich[1,*] and Duane D. Johnson[1,2,*]

[1]*Ames Laboratory, U.S. Department of Energy at Iowa State University, Ames, Iowa 50011-3020, USA*
[2]*Department of Materials Science and Engineering, Iowa State University, Ames, Iowa 50011-2300, USA*

Nitinol (NiTi), the most widely used shape-memory alloy, exhibits an austenite phase that has yet to be identified. The usually assumed austenitic structure is cubic B2, which has imaginary phonon modes, hence it is unstable. We suggest a stable austenitic structure that "on average" has B2 symmetry (observed by x-ray and neutron diffraction), but it exhibits *finite* atomic displacements from the ideal B2 sites. The proposed structure has a phonon spectrum that agrees with that from neutron scattering, has diffraction spectra in agreement with x-ray diffraction, and has an energy relative to the ground state that agrees with calorimetry data.

I. INTRODUCTION

Nitinol (NiTi) is among the most used industrial shape-memory alloys [1–3]. The shape-memory effect versus temperature (T) is associated with a transformation between the high-T austenite and low-T martensite phases. The B2 structure [CsCl with $Pm\bar{3}m$ space group no. 221; see Fig. 1(a)] suggested for the high-T austenite phase by x-ray diffraction (XRD) and neutron scattering experiments on powder [4,5] is found theoretically to have unstable phonons [6–8]. Hence, B2 NiTi cannot be the actual structure. Yet neutron scattering measurements [9] find a stable phonon spectrum for the austenite phase. From single-crystal x-ray diffraction (XRD) and transmission electron microscopy (TEM) experiments, the austenitic structure deviates from B2 [2,10], especially at lower T, and it was described as a premartensitic instability [10]. Therefore, determining the structure of austenite is paramount to understanding NiTi phase stability and transformations, including those associated with shape-memory.

Here we predict a stable austenitic structure (Fig. 1), which agrees with known data from neutron scattering and calorimetry [9,11], as well as XRD [2,5,10,11]. Intriguingly, this structure has *large* atomic displacements from the ideal B2 sites, up to 22% of the B2 lattice constant at 0 K—above that suggested by the Lindemann criterion [12] for melting. This predicted austenitic structure cannot be described by B2 symmetry, although in diffraction it appears B2 on average [Fig. 1(b)]. Here we describe only one stable representation of the austenite phase, with many other similar states possible, as found for phonon glass behavior (see Fig. 42 in Ref. [13]), all of which have similar energy per atom and atomic distribution functions. Increasing the unit cell and considering other representative stable structures does not change our general results.

From density-functional theory (DFT), the NiTi ground-state structure is base-centered orthorhombic (BCO) [14,15], while the experimentally assessed structure is monoclinic B19′, a low-energy deformation of the BCO ground state [2,14]. In DFT, the previously considered ideal B2 ↔ BCO transformations [16,17] have no barrier. For ideal B2, the XRD pattern actually differs from those measured [2,10,11]. In addition, from previous and present DFT results, the B2

energy relative to BCO is 48 meV/at (557 K), much too high compared to the observed $T_c \approx 313$ K [11]. Because the ideal B2 phase has multiple unstable phonon modes (Fig. 2), one can expect multiple nearby local energy minima, all with similar energies. Lastly, single-crystal diffraction data suggest evidence that NiTi austenitic structure was not a simple B2, as believed based on powder diffraction; rather it has a 9.03 Å superlattice and a ∼ 3 Å sublattice [2,10], i.e., a 3×3×3 set of two-atom B2 cells, containing 54 atoms. This structure was not identified.

II. AUSTENITIC STRUCTURE

To find a stable NiTi austenite, we investigated cells of increasing size with B2 chemical order that permitted symmetry breaking by atomic displacements. We chose a 54-atom hexagonal unit cell with the c-axis along B2 $\langle 111 \rangle$, and two ∼9 Å basal plane vectors along B2 $\langle \bar{1}01 \rangle$ and $\langle 0\bar{1}1 \rangle$. Its unit cell vectors $(\bar{a},\bar{b},\bar{c})$ in terms of $(\bar{x},\bar{y},\bar{z})$ for cubic B2 are $\bar{a}=3(\bar{z}-\bar{x})$, $\bar{b}=3(\bar{z}-\bar{y})$, and $\bar{c}=\bar{x}+\bar{y}+\bar{z}$. Using *ab initio* molecular dynamics (MD) followed by relaxation at 0 K to a local energy minimum, we obtain a stable austenitic $Ni_{27}Ti_{27}$ structure [Figs. 1(c) and 1(d)]. This hexagonal structure (Fig. 1) has a c/a ratio of 0.3954, which is a 3% reduction compared to c/a of 0.4082 (i.e., $1/\sqrt{6}$) for our unit cell with ideal B2 order, where $c = a_{B2}\sqrt{3}$ and $a = 3a_{B2}\sqrt{2}$ in terms of $a_{B2} = 3$ Å.

Our austenitic structure has a DFT energy ΔE of 29 meV/at (340 K) above BCO, in better agreement [18] with the measured T_c for equiatomic NiTi of 313 K [11]. Typically [18], $\Delta E \approx k_B T_c$, which provides reliable estimates of phase-transition temperatures [19], especially for magnetic transitions. From the ΔE and estimated entropy difference of $1/2\,k_B$ per atom [9] for the martensite-to-austenite transformation, we predict [20] the latent heat to be below 15 meV/at (1.4 kJ/mol) at T_c, while the calorimetry values are 1.07 ± 0.10 kJ/mol (cooling) and 1.3 ± 0.2 kJ/mol (heating) [9]. Thus, the calculated thermodynamic quantities closely reproduce the measured values.

III. COMPUTATIONAL DETAILS

To predict this structure, we used a plane-wave pseudopotential-based DFT method using the generalized gradient approximation (GGA) [21] and a projected
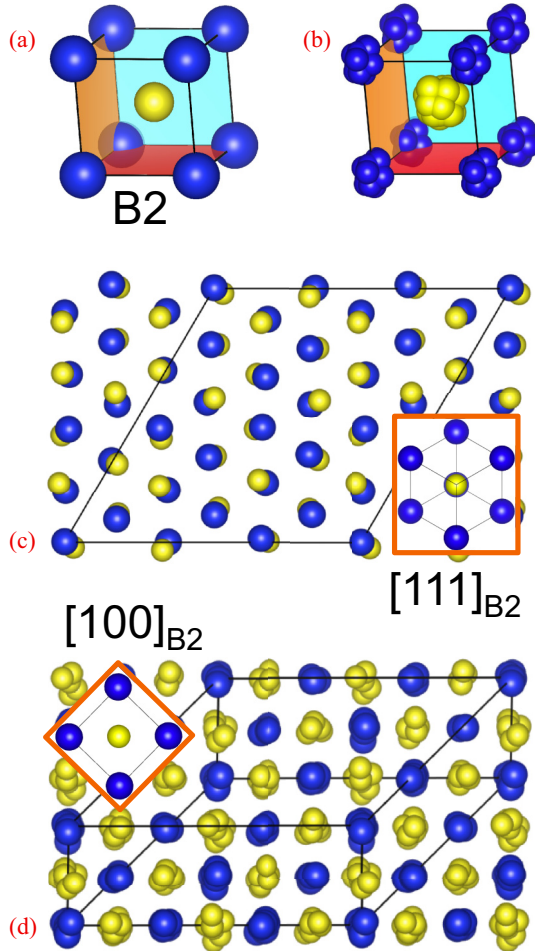
————
*zarkev@ameslab.gov; ddj@ameslab.gov

FIG. 1. (Color online) Atomic structure of the $Ni_{27}Ti_{27}$ austenite, compared to B2, with Ni (yellow) and Ti (blue) atoms. (a) Ideal B2. (b) Projection of $Ni_{27}Ti_{27}$ atomic positions onto a B2 cell. (c) Hexagonal [0001] projection, compared to $[111]_{B2}$. (d) Viewed along $[100]_{B2}$.

augmented wave (PAW) basis [22], as implemented in VASP code [23,24] with convergence obtained by a second Broyden's method [25]. We choose a 337 eV plane-wave energy cutoff and a 544.6 eV augmentation charge cutoff. We converged total energies and forces using k-meshes with at least 50 k-points per $Å^{-1}$ (e.g., $11\times13\times17$ for a $4.92\times4.00\times2.92$ Å cell). The structure of the high-T phase in a 54-atom $Ni_{27}Ti_{27}$ cell is investigated using *ab initio* MD with 1 fs time steps in a Nosé thermostat. After 1000 fs at 800 K, temperature was quenched from 800 to 0 K in 800 fs; next, the atoms were relaxed using the conjugate-gradient algorithm. We performed an internal atomic relaxation in a large fixed unit cell, and then a full relaxation of both atoms and lattice vectors. Lastly, phonon spectra were constructed using the calculated atomic forces for 162 independent 0.04 Å displacements in a 108-atom $1\times1\times2$ hexagonal supercell (only two independent atomic displacements in a 54-atom $3\times3\times3$ cubic supercell for B2) within the small displacement method in the PHON code [26]. We have checked that the PHONOPY code [27] gives the same results.

Phonons at finite T (Fig. 2) are addressed by combining three codes: VASP [23,24], THERMOPHONON [28], and
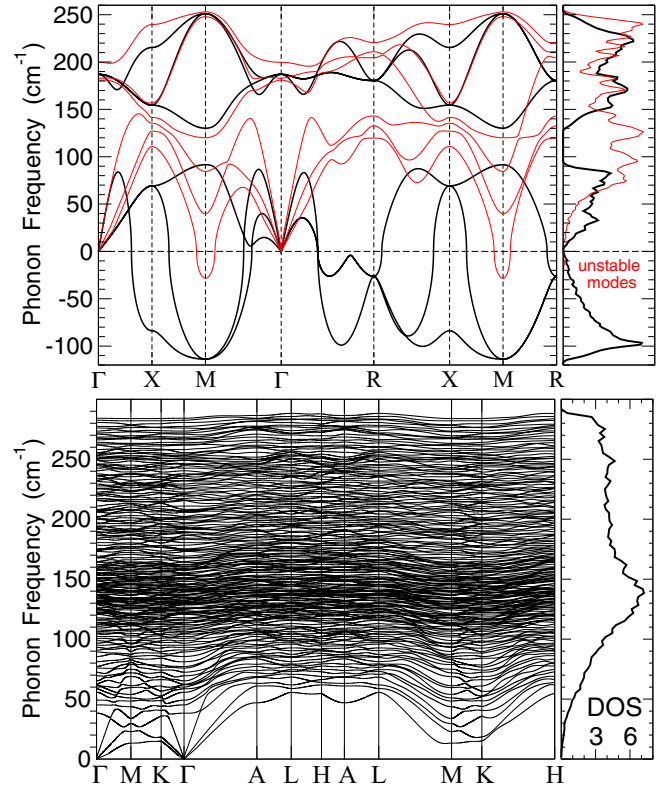

FIG. 2. (Color online) Calculated phonon spectra and density of states (DOS) of (upper) ideal B2 at 0 K (black) and 1586 K (red) with unstable negative phonon frequencies and (lower) new austenitic structure (stable), with DOS units of 10^{-3} states/cm^{-1}.

PHONOPY [27]. First, an *ab initio* MD in a 54-atom, $3\times3\times3$, $(9 \text{ Å})^3$ cubic supercell with Nosé thermostat at a given T with 1 fs time steps is used to obtain atomic positions and forces for over 50 000 fs steps after 2000 fs equilibration. Next, force constants are calculated using our THERMOPHONON code [28] in the assumption of ideal B2 average atomic positions, and used in PHONOPY [27] with symmetrization to construct the phonon spectrum from the *ab initio* MD data. We performed MD calculations at a range of T, including 0, 300, 800, 1200, and 1586 K (melting), and we found that although already at 300 K the instability is only around M, and its relative weight decreases with T, this instability survives at all T up to melting.

IV. DISCUSSION

For the proposed austenitic structure, the calculated 0 K phonon spectrum is stable (Fig. 2), in contrast to ideal B2. Also, as we have confirmed up to 1586 K (experimental melting temperature), vibrational entropy does not stabilize ideal B2, see Fig. 2, where the M point remains always unstable at high temperatures. More compellingly, the calculated phonon density of states (DOS) of the predicted austenite phase (Fig. 2) agrees well with that found from neutron scattering [9], as shown directly in Fig. 3.

Interestingly, this predicted austenitic structure, with atoms displaced from the perfect B2 positions, looks like B2 on average [Fig. 1(b)]. The simulated XRD pattern at 0 K is
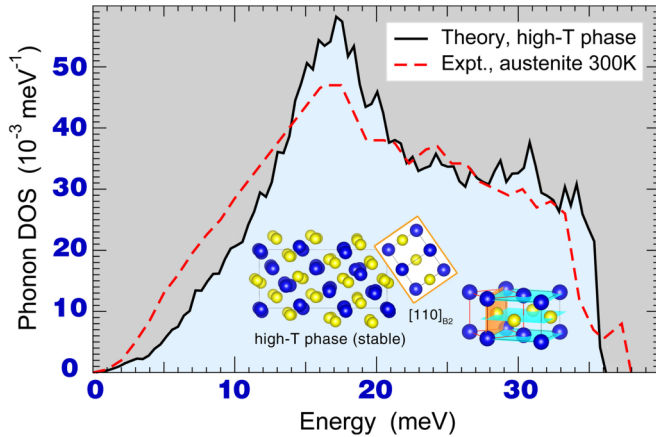
FIG. 3. (Color online) Austenite phonon DOS from theory (new structure, see the lower figure in Fig. 2) and neutron diffraction experiment [9]. Experimental error bar below 10 meV is ± 4 meV. Inset: austenitic structure (left) compared to ideal B2 (right) and its $[110]_{B2}$ projection (center).

FIG. 5. (Color online) The NN-pair distribution function in the fully relaxed austenitic structure (atomic coordinates are in Table S1). The binning size is 0.04 Å. The NN distance in ideal B2 structure is 2.6 Å (vertical dashed line); dotted lines show $\pm 5\%$ deviations. Inset: Ni (yellow) and Ti (blue) positions projected onto a B2 cell [see Fig. 1(b)].

shown in Fig. 4. With all B2 peaks still present, this pattern does not contradict any previous experimental XRD data. The additional XRD peaks can be at various positions for different local energy minima in the austenite phase; in this case, they contribute to the background after summation.

Further details of the structure offer additional insight, and potential comparison to pair distribution functions from new diffraction experiments. From the calculated pair distribution function, the nearest-neighbor (NN) distances have a distribution (Fig. 5) with <5% half-width from the 2.6 Å NN distance in B2 (2.43–2.88 Å). In the Supplemental Material [29], we provide the atomic direct lattice coordinates (Table S1) in our representation of the austenite unit cell. From these data, we plot the NN-pair distribution function (Fig. 5) and the atomic displacements relative to the ideal B2 positions (Fig. 6).
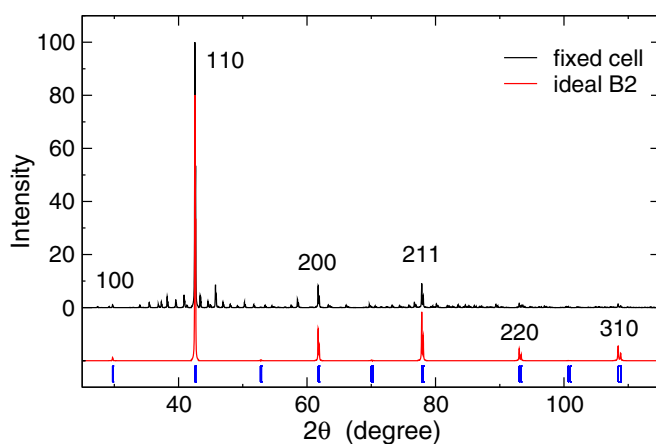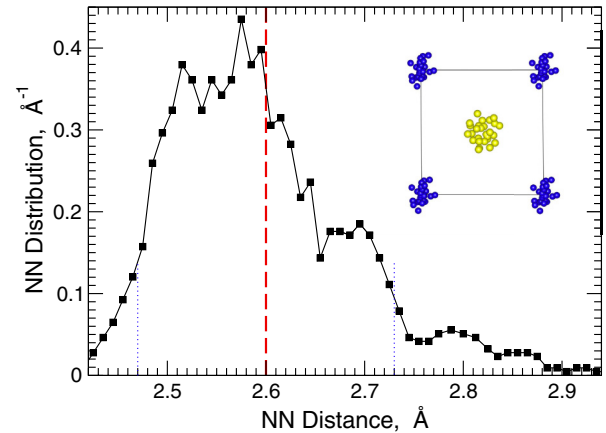
V. SUMMARY

In summary, there is a multiplicity of solutions to our original question: "What is the stable structure of NiTi austenite?" We have proposed a stable representative structure (one of many) for the high-T NiTi austenite phase, whose energy relative to the BCO ground state, diffraction spectra, and vibrational density of states agree, respectively, with available calorimetry, XRD, and neutron scattering data, whereas those of an ideal (unstable) B2 do not. We suggest new experiments to assess the inherent displacement in NiTi austenite, with a large Debye-Waller factor at low temperatures (not the usual thermal disordering from phonons). We are assessing the solid-solid martensitic transformation paths for NiTi [17].

FIG. 4. (Color online) Simulated XRD spectrum of our proposed austenitic structure (black) compared to ideal B2 (red).
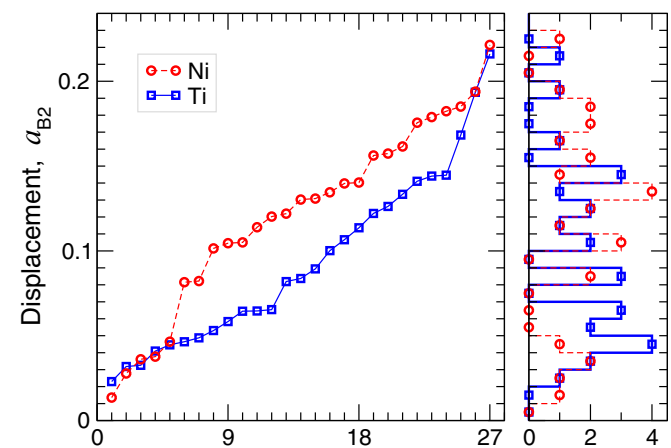

FIG. 6. (Color online) Displacements from ideal B2 positions (sorted by magnitude) of the relaxed atoms in a fixed hexagonal $Ni_{27}Ti_{27}$ unit cell. Right panel: Number of displaced atoms per 0.03 Å bin, where the largest value (0.66 Å) is 25% of the NN distance and 22% of the lattice constant in ideal B2, $a_{B2} = 3$ Å.

[1] W. J. Buehler, J. W. Gilfrich, and R. C. Wiley, J. Appl. Phys. **34**, 1475 (1963).

[2] F. E. Wang, W. J. Buehler, and S. J. Pickart, J. Appl. Phys. **36**, 3232 (1965).

[3] V. M. Danilenko, G. M. Lukashenko, and S. B. Prima, Sov. Powder Metall. Met. Ceram. **30**, 412 (1991) [Poroshkov. Metallurg. **5**, 70 (1991)].

[4] M. J. Marcinkowski, A. S. Sastri, and D. Koskimaki, Philos. Mag. **18**, 945 (1968).

[5] F. E. Wang, S. J. Pickart, and H. A. Alperin, J. Appl. Phys. **43**, 97 (1972).

[6] G. L. Zhao and B. N. Harmon, Phys. Rev. B **48**, 2031 (1993).

[7] X. Y. Huang, C. Bungaro, V. Godlevsky, and K. M. Rabe, Phys. Rev. B **65**, 014108 (2001).

[8] N. Hatcher, O. Y. Kontsevoi, and A. J. Freeman, Phys. Rev. B **79**, 020202(R) (2009).

[9] P. D. Bogdanoff and B. Fultz, Philos. Mag. B **81**, 299 (2001).

[10] G. D. Sandrock, A. J. Perkins, and R. F. Hehemann, Metallurg. Trans. **2**, 2769 (1971).

[11] R. Schmidt, M. Schleretht, H. Wipf, W. Assmus, and M. Müllner, J. Phys.: Condens. Matter **1**, 2473 (1989).

[12] F. A. Lindemann, Z. Phys. **11**, 609 (1910).

[13] T. Takabatake, K. Suekuni, T. Nakayama, and E. Kaneshita, Rev. Mod. Phys. **86**, 669 (2014).

[14] X. Huang, G. J. Ackland, and K. M. Rabe, Nat. Mater. **2**, 307 (2003).

[15] K. G. Vishnu and A. Strachan, Acta Mater. **58**, 745 (2010).

[16] S. Kibey, H. Sehitoglu, and D. D. Johnson, Acta Mater. **57**, 1624 (2009).

[17] N. A. Zarkevich and D. D. Johnson (unpublished, 2014).

[18] N. A. Zarkevich, Ph.D. thesis, University of Illinois, Urbana-Champaign, 2003. Permanent URL http://hdl.handle.net/2142/34849, see Eq. 3.7 on p. 33.

[19] A. Alam, B. Kraczek, and D. D. Johnson, Phys. Rev. B **82**, 024435 (2010).

[20] N. A. Zarkevich and D. D. Johnson, Phys. Rev. Lett. **100**, 040602 (2008).

[21] J. P. Perdew, Phys. Lett. A **165**, 79 (1992).

[22] P. E. Blöchl, Phys. Rev. B **50**, 17953 (1994).

[23] G. Kresse and J. Furthmüller, Comput. Mater. Sci. **6**, 15 (1996).

[24] G. Kresse and J. Furthmüller, Phys. Rev. B **54**, 11169 (1996).

[25] D. D. Johnson, Phys. Rev. B **38**, 12807 (1988).

[26] D. Alfé, Comput. Phys. Commun. **180**, 2622 (2009).

[27] A. Togo, F. Oba, and I. Tanaka, Phys. Rev. B **78**, 134106 (2008).

[28] N. A. Zarkevich, THERMOPHONON code (2014).

[29] See Supplemental Material at http://link.aps.org/supplemental/10.1103/PhysRevB.90.060102 for the atomic direct lattice coordinates (Table S1) in our representation of the austenite unit cell.